Dynamics of double-knotted DNA molecules under nanochannel confinement

Runfang Mao and Kevin D. Dorfman*

Department of Chemical Engineering and Materials Science, University of Minnesota - Twin Cities, 421 Washington Ave. SE, Minneapolis, MN, USA

E-mail: dorfman@umn.edu

*To whom correspondence should be addressed

Abstract

Langevin dynamics simulations of double-knotted DNA molecules in a nanochannel reveal that the interactions between the two knots differ with degree of channel confinement. In relatively wide channels, the two knots can intertwine with each other, forming a persistent, intertwined knot. Moreover, the two knots are able to pass through each other in large channels. In contrast, for small channel sizes, the knots tend to remain separated, and their crossing is inhibited. The change in knot-knot interactions as channel size decreases is rationalized through an analysis of the magnitude of the transverse fluctuations, which must be large enough to allow one knot to swell to accommodate the intertwined state.

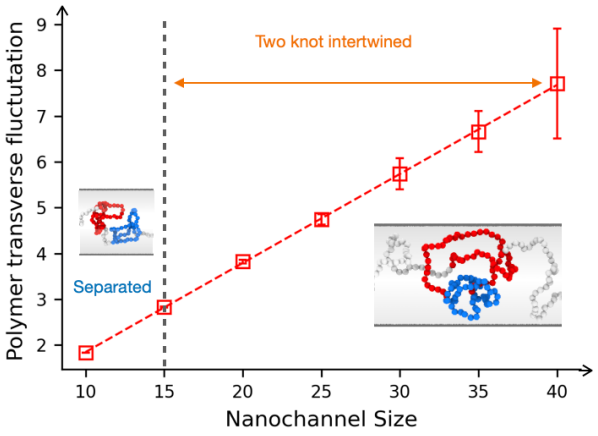

Introduction

DNA has proven to be a powerful model system for investigating polymer physics and self-entanglement, in particular the dynamics of knots along a polymer chain,[1–3] owing to the ability to visualize the knot dynamics via fluorescence microscopy and methods to reliably produce (pseudo)knots along linear DNA molecules. Linear DNA cannot be knotted in a topological sense because it has free ends. Rather, it supports pseudoknots that are destroyed by diffusion to those chain ends. We will follow the convention in the literature and refer to these objects as knots, suppressing the distinction between a true knot and a pseudoknot. One approach to create DNA knots uses optical tweezers,[4,5] and knots also can be formed and analyzed under flow in microfluidic devices[6–8] or using confinement-induced chain self-entanglement and compaction.[9] In addition to their utility as a model system for polymer physics, understanding the properties of DNA knots has important implications for biology[10–13] because knots form sporadically when long, loose DNA molecules experience random cyclization.[12] Moreover, an elaborate topoisomerase machinery exists to regulate the topological state of DNA in cells because the presence of a DNA knot exerts a significant influence on the mechanical and dynamic properties of the polymer, with important implications for critical biological processes like cell replication and transcription.[14–16] Knot formation also detrimentally affects the precision of sequence detection techniques, particularly within the context of genome mapping in modern biotechnological applications.[17,18]

Most previous studies of DNA knots focused on analyzing the dynamics of single knots along the chain.[8,19–21] However, DNA also exhibits a tendency to form two knots,[22–24] a phenomenon particularly prevalent in the so-called knot factory.[9,25] Prior research indicates that the presence of a second knot significantly alters the knot dynamics. While both knots follow the conventional untying processes as they approach the chain ends, two proximate knots undergo a distinctive process involving attractive interactions[26–30] that bring the two knots together and ultimately leads to intertwining, especially when the polymer is under tension. Computational work confirmed such behavior and showed that two knots can be

intertwined, passing through each other by swapping positions.[27] In stark contrast, when subjected to nanochannel confinement, experiments indicate that two knots do not seem to experience an apparent attraction.[9,25] Instead, they prefer a relatively stable, separated state. Likewise, these nanochannel experiments showed that two knots remain in close contact for only several seconds,[25] in contrast to the close proximity of several minutes observed under electrokinetic flow-induced stretching.[26]

These distinctly different behaviors between the dynamics of two knots on stretched DNA versus channel-confined DNA prompted us to investigate in more detail how confinement influences the interactions between two knots along a DNA molecule. Experiments are challenging in this respect because they do not permit ready control (nor a direct measurement) of the knot type,[25] and they lack the spatial resolution required to analyze the knot in detail, in particular to distinguish between intertwined knots and two knots in close proximity. Moreover, changing the degree of confinement requires either changing the channel size or the ionic strength of the system, the latter affecting the persistence length and effective width of the DNA.[31] Neither of these approaches to vary the confinement are straightforward experiments. Fabricating an array of square channels of different sizes is a costly endeavor. Confinement spectroscopy, using a funnel-shaped channel of fixed depth provides a way to efficiently change the effective channel size,[32–34] but the use of rectangular channels complicates the analysis of the system.[33,35] Finally, while it is relatively straightforward to adjust the ionic strength of the buffer, this approach simultaneously changes the polymer properties governing the tightness of the knots[36] and the degree of confinement, which confounds the analysis.

The most straightforward way to understand the role of confinement on the interaction between two knots is by simulation. To this end, the present contribution reports Langevin dynamics simulations that probe the interactions and dynamics of nanochannel-confined DNA molecules containing two knots. By tracking the knot size and position along the DNA molecule over time, we gain insights into the time evolution of the two-knot structures,

including the probability of achieving an intertwined state. We also analyze the interaction between the two knots by calculating the free energy profile as a function of knot-knot separation distance and the probability of being in the intertwined state, allowing us to understand the impact of channel size on the behavior of the two knots. Notably, while we find that two knots can intertwine and pass through each other under modest nanochannel confinement, a small channel size serves as a restriction parameter, inhibiting the intertwining and crossing of two separated knots. We explain this behavior through an analysis of the changes in the transverse fluctuations of the double-knotted chain when it is confined, and show that it is not related to the ability to form a global hairpin.

Methods

Polmer model

The knotted DNA molecule is modeled using a standard spring-bead model.[20,27] Adjacent beads i and j are connected via finite extensible nonlinear elastic (FENE) bond,[37]

$$U_{\mathrm{FENE}} = -0.5 k_{\mathrm{bond}} R_0^2 \ln\left[1 - \left(\frac{r_{ij}}{R_0}\right)^2\right], \quad r_{ij} \leq R_0 \tag{1}$$

where $R_0 = 1.5\sigma$ is the maximum bond length in terms of the length scale σ, $k_{\mathrm{bond}} = 30$ $k_{\mathrm{B}}T$ denotes the stiffness of the bond, k_{B} is the Boltzmann constant, T is the temperature, and r_{ij} is the distance between bead i and j. The non-bonded pairwise interaction between beads is represented by the purely repulsive Weeks-Chandler-Andersen (WCA) potential,[38]

$$U_{\mathrm{WCA}} = \begin{cases} 4\epsilon\left[\left(\dfrac{\sigma}{r_{ij}}\right)^{12} - \left(\dfrac{\sigma}{r_{ij}}\right)^{6}\right] + \epsilon, & r \leq 2^{1/6}\sigma \\ 0, & r > 2^{1/6}\sigma \end{cases} \tag{2}$$

where $\epsilon = k_{\mathrm{B}}T$. The rigidity of the chain is expressed via an angle potential,

$$U_{\mathrm{angle}} = 0.5k_{\mathrm{bend}}(\theta_i - \pi)^2 \tag{3}$$

where θ_i is the angle formed by three contiguous beads. The bending penalty, $k_{\mathrm{bend}} = 5$ $k_{\mathrm{B}}T$, corresponds to a DNA in a buffer solution with an ionic strength of 18 mM,[25] with persistence length $l_p = 60$ nm using a bead diameter $w = \sigma = 12$ nm using the relationship[18]

$$\frac{l_p}{w} = \frac{k_{\mathrm{bend}}}{k_{\mathrm{bend}} - k_{\mathrm{bend}}\coth(k_{\mathrm{bend}}) + 1} \tag{4}$$

Confinement within a nanochannel is enforced along the y- and z-axis using a wall potential, expressed via the WCA potential

$$U_{\mathrm{wall}} = \begin{cases} 4\epsilon\left[\left(\dfrac{\sigma}{d_i}\right)^{12} - \left(\dfrac{\sigma}{d_i}\right)^{6}\right] + \epsilon, & d_i \leq 2^{1/6}\sigma \\ 0, & d_i > 2^{1/6}\sigma \end{cases} \tag{5}$$

where d_i is the orthogonal distance between bead i and wall.

Knot initial configuration

The initial configuration of nanochannel-confined, double-knot DNA molecules was generated in two parts: the relaxed, unknotted DNA and the trefoil 3_1 knot part, following similar procedure as our previous work.[20] The first part involves creating a relaxed, nanochannel-confined DNA molecule with a contour length of $L_c = 300\sigma$ via a short molecular dynamics simulation. The second part includes a relatively tight, right-handed, 3_1 trefoil knot configuration, generated by Knotplot,[39] containing 17 beads within the knotted portion. The double-knot DNA molecule configuration was formed by inserting the right-handed trefoil knots at 1/3 and 2/3 of the contour length of the relaxed DNA molecule. Figure 1 shows a schematic of the double-knot DNA molecule confined in a nanochannel with channel width

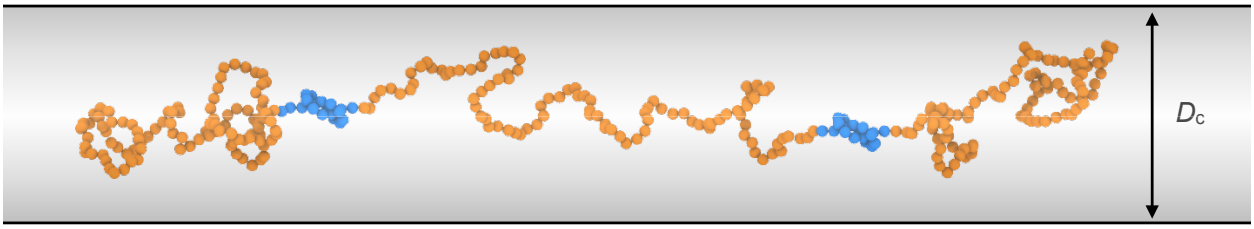

Figure 1: Schematic of the initial configuration of a double-knot DNA molecule under nanochannel confinement. The knotted and unknotted parts are indicated by the blue and orange color, respectively.

$D_c/\sigma = 15$. We also generated the initial configuration for double-knot DNA molecule with 4_1 knot, following the same approach described above.

Molecular dynamics simulation details

Molecular dynamics simulations were conducted to investigate the behavior of double-knot DNA molecules under nanochannel confinement using LAMMPS.[40] A Langevin thermostat, with a damping coefficient $\tau = 2$ was utilized to maintain the thermostat of a canonical ensemble (NVT). The DNA molecules, each having two knots, were placed initially at the center of the simulation box, with a size of $300 \times D_c \times D_c$, where D_c denotes the channel width along the y- and z-directions. A total of seven channel sizes with $D_c/\sigma = 10$, 15, 20, 25, 30, 35 and 40 were studied. A periodic boundary condition was applied in the x-direction, while the wall potentials in Eq. 5 were applied along the y- and z-directions to enforce confinement. Each simulation was conducted with total of 2×10^4 τ_{MD} for production after local energy minimization of the geometries of double-knot DNA molecules. In this context, $\tau_{MD} = \sigma(m/\epsilon)^{1/2}$ denotes the Lennard-Jones (LJ) time. The simulations were performed isothermally at a reduced temperature, $T^* = 1$. All quantities are represented in LJ reduced units, and all particle beads have equal masses, $m = 1$. The simulation configurations were dumped every 10 τ_{MD} for subsequent analysis. For each channel size, at least 300 different double-knot DNA configurations were generated and then simulated.

Knot identification

The knot structure of DNA molecules was identified by calculating the Alexander polynomial of the localized knots via Kymoknot.[41] For linear chains, it is possible to establish the pseudoknot structure by bridging the two terminal ends of the DNA molecules. Consequently, the knot structure from a pseudo-closed ring can be discerned as a well-defined topological state. We utilized a bottom-up approach capable of localizing the knot portion on a linear chain, which involves searching for the knot start and end position from short sections of the molecule, gradually extending to longer ones. The knot was identified when the subchain used in the knot calculation exhibits a physical knot similar to the entire chain, while the remaining parts were physically unknotted.[41]

The localization of the relative positions of two knots requires the determination of the starting and ending positions for each knot. As a first screening step, the entire DNA molecule was analyzed to (i) check if the chain was likely to contain two knots and (ii) provide an initial guesses for the starting and ending points for the two knots; the analysis of the entire molecule produces a complex knot that must contain within it the two trefoil knots. For the first knot, knot 1, the initial starting point was defined as the left terminal end of the DNA molecule, i.e., bead index of 0. We used the starting point searched from first screening step as the initial ending point for knot 1, and the ending point was gradually extended during the search for a longer portion of the DNA molecule, with an interval of 10 bead indices per step. At each step, the Alexander polynomial was calculated to confirm the knot type and the start/end beads for that knot within the DNA. The search was terminated early when the Alexander polynomial already corresponds to a trefoil knot structure or it reached the ending position of the complex knot. The analysis ultimately furnishes the fractional contour position for the start, K_{1s}, and end, K_{1e}, of the first knot (Fig. 2a). A similar approach can be used to localize the second knot, knot 2, with the starting point defined as the right terminal end of the DNA molecule, and the ending point gradually moved towards the left side of the longer portion of the DNA molecule. The result of this

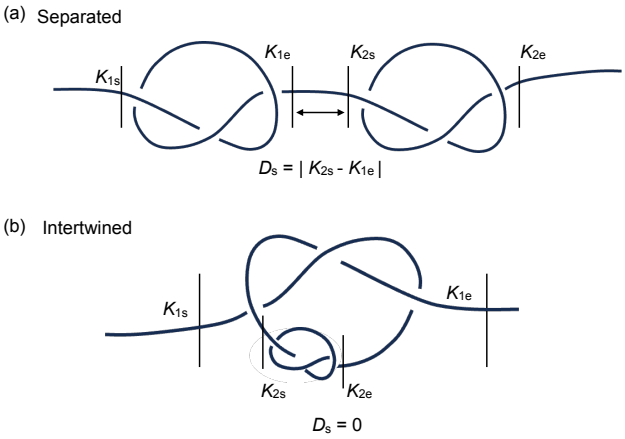

Figure 2: Knot identification schematic. (a) Two separated knots with identified knot starting position K_{1s} and K_{2s} and ending position K_{1e} and K_{2e} for knot 1 and knot 2, respectively. The separation distance D_s is the fraction of the total contour length contained between the the two knots. (b) The intertwined state of two knots. Two knots are considered as intertwined when the number of overlapping bead indices between knot 1 and knot 2 is greater than 10. For an intertwined knot, the separation distance is set as 0.

second analysis is the starting and ending fractional contour positions of the second knot, $K_{2\mathrm{s}}$ and $K_{2\mathrm{e}}$ (Fig. 2a).

Throughout the simulations, it was observed that the two knots can be either in "separated" or "intertwined" states, respectively. The "separated" state (Fig. 2a) is thus defined as cases when the number of overlapping bead indices between the two knots is less than 10. Otherwise, the chain is in the "intertwined" state (Fig. 2b). When the knots are separated, the separation distance, D_s, is thus defined as the fraction of the total DNA contour length that is contained between the two knots (Fig. 2a). In the intertwined state, the separation distance between the two knots is set to 0. For all other cases, where the entire molecule only produces a single trefoil knot or no knot at all, it simply means that the chain does not contain two knots and the separation distance is no longer applicable.[20] Note that the definition of $D_s = 0.0$, i.e., the intertwined state, in our simulation differs from that used in experimental studies,[25,26] where knots are considered to be in close proximity. To compare with experimental studies, a larger separation distance cutoff may be required to classify them as in close proximity when using the dataset collected in our simulation.

Free energy calculation

The free energy as a function of the separation between two knots can be computed from the observed probability distribution for that distance,

$$F(D_s) = -k_B T \ln[P(D_s)] \tag{6}$$

where $P(D_s)$ is the normalized probability distribution of the knot separation distance, D_s, collected from all parallel simulations. The $P(D_s)$ distribution includes all samples, regardless of whether the two knots approach each other or remain far apart. This analysis is restricted to the case $D_s > 0$ since all of the intertwined states are, by our definition, degenerate with a single value $D_s = 0$. Across all parallel simulations, the probability that the two knots do not meet until untied is approximately 30% (see Fig. S1).

Transverse fluctuation

The lateral displacement y_i is the displacement in the y-direction that is perpendicular to the nanochannel axis, namely x-axis. The fluctuations are only moderately impacted by the channel walls,[42] so we estimated the variance in the transverse position from the variance in the y-position,

$$\sigma_\perp^2 = \frac{1}{N} \sum_{i=1}^{N} y_i^2 \tag{7}$$

Unconfined simulations

We will also present data for unconfined, stretched DNA. In these simulations, the nanochannel wall potential in Eq. 5 was removed. Each of the two terminal ends of DNAs was tethered to a region near its initial position using the `fix spring` command in LAMMPS, which applies the stiff harmonic potential,

$$U_{\text{spring}} = 0.5 k_{\text{spring}} (r - r_0)^2 \tag{8}$$

where $k_{\text{spring}} = 20\epsilon/\sigma^2$ is the spring constant, with $r_0 = 1.5\sigma$ as the equilibrium distance from tether point. This constraint with non-zero offset r_0 allows more mobility for the chain ends, which we posit provides a better mimic of the nanochannel-driven extension than tethering to a single point. This approach allows the double-knotted, unconfined DNA molecules to exhibit a similar average chain extension and variance as those confined in nanochannels at different nanochannel sizes, as shown in Fig. S2. There are minor differences between the two cases, but these will prove irrelevant to our analysis.

The initial conditions for these simulations are not necessarily aligned with the x-axis because they are based on the initial configuration of the nanochannel-confined DNA. To use Eq. 7, rotational transformation matrices were applied to project the DNA end-to-end vector to the x-axis. In the unconfined case, the fluctuations are expected to have circular symmetry.

Results

In general, we observed two different types of behavior in the simulations. Figure 3a,b provides an example of the first type, demonstrating attraction and intertwining of two knots before they eventually untie by reaching the chain ends. These dynamics are similar to what has been previously observed[26,27] in stretched, knotted polymers. When two initially separated knots approach each other, the two knots come in close contact and stay intertwined for a long duration. Before intertwining, a sudden expansion of one of the trefoil knots is observed, which allows it to accommodate the other knot. Additionally, the trefoil knot is contained within the intertwined knot, moving along it throughout the entire intertwined state. The escaped knots have the same knot type as when they entered the intertwined state. Throughout this period, no transformation in the type of knots was observed. The second type of behavior is illustrated by Fig. 3c,d, where two initially separated knots can also maintain a separated state and untie by diffusing towards the ends of the chain sepa-

rately, as shown in Figure 3c. In contrast to the swelling observed prior to the intertwined case, Fig. 3d provides an example where the two knots stay relatively compact when they come into close proximity.

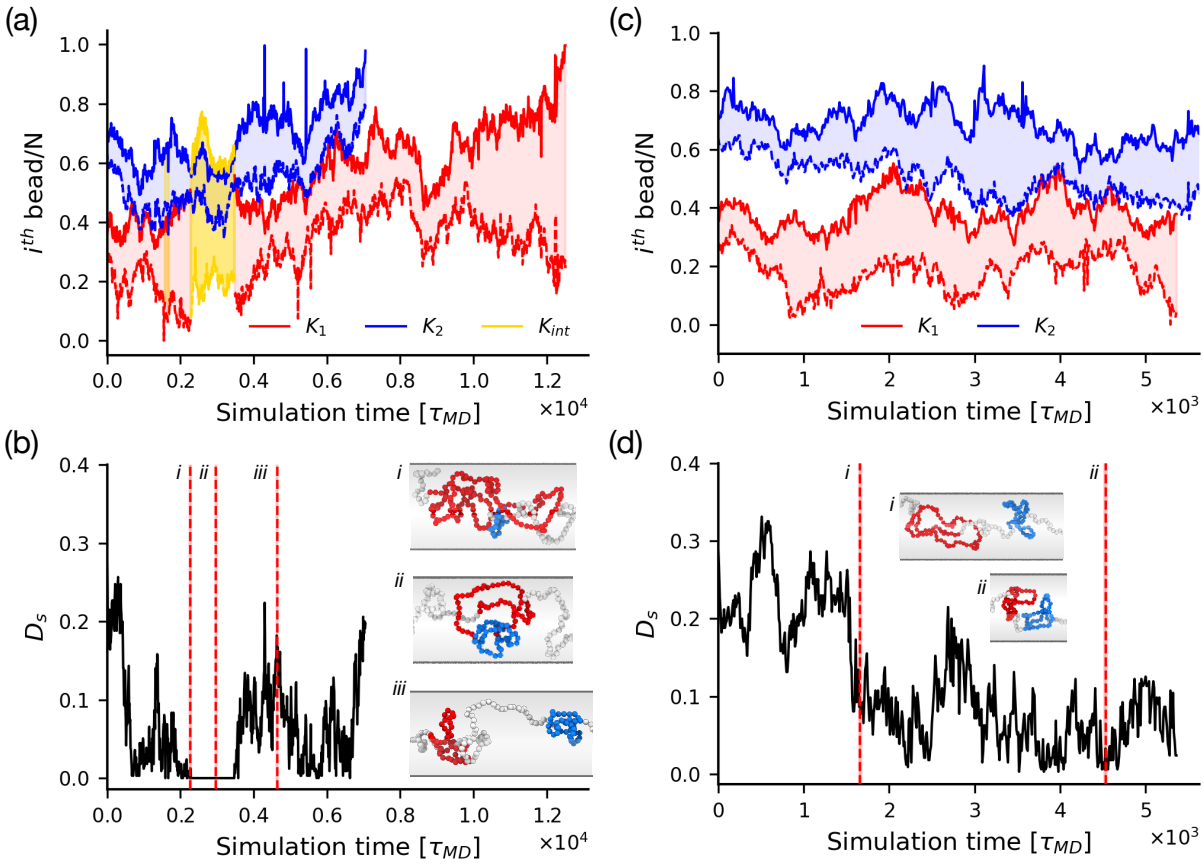

Figure 3: Time evolution of a double-knot DNA molecule inside a 15σ wide channel, showing two knots can become intertwined (a,b) or remain separated (c,d) from each other. (a,c) Knot position, representing the identified knot indices normalized with the total chain contour length N, as a function of simulation time. The blue and red regions indicate the knot positions for knot 1 and knot 2, respectively, while the yellow region highlights the intertwined state, which corresponds to a single complex, intertwined knot. The dashed and solid lines represent the starting and ending position for knot 1 (red), knot 2 (blue) and the intertwined knot state (yellow), respectively. (b,d) The knot-knot separation distance, D_s, as a function of simulation time in terms of the knot location given in panel (a,c). The insets show the knot configurations at the different times indicated by the vertical, dashed red lines. The red and blue colors for the beads in the insets are knot 1 and knot 2, respectively, in panels (a,c).

The data for the values of D_s as a function of simulation time in Figs. 3b and 3d, when averaged over all of the replicates, provide a probability density $p(D_s)$ that can be used to

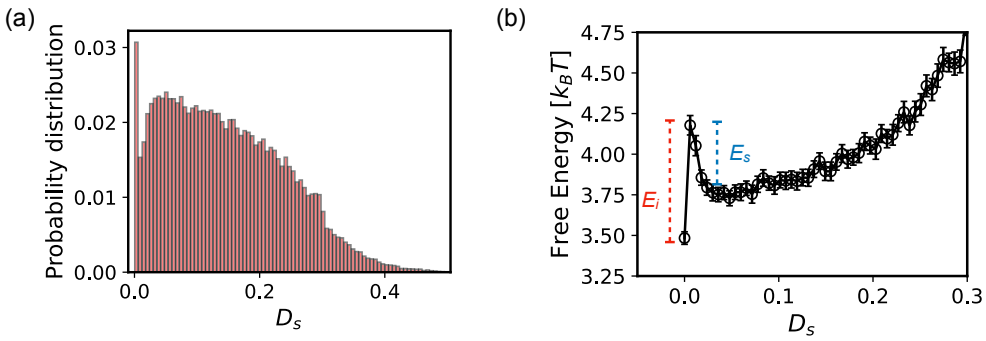

Figure 4: Free energy profile derived from the probability distribution function. (a) Probability distribution of knot-knot separation distance, D_s, at $D_c/\sigma = 30$. (b) Free energy profile as a function of knot-knot separation distance. The free energy barrier E_s is the energy difference between the local maximum at the transition state and the local minimum where the knots are close to the transition state. The free energy barrier E_i is the free energy difference between the transition state and the intertwined knot state. The $x-$axis is truncated at 0.3 to highlight the two barriers.

compute the free energy as a function of D_s from Eq. 6. Figure 4 shows an example of such a free energy calculation of a double-knot DNA molecule inside a 30σ wide channel. In principle, one could extract two free energy barriers from data of the type in Fig. 4, one for the transition between the separated state and the transition state, E_s, and the other for the transition between the intertwined state and the transition state, E_i in a manner analogous to what was done in experimental measurements of two knots for nanochannel-confined DNA.[25] However, neither of these estimates are reliable due to the challenges in defining an intertwined state. To say that the two knots are intertwined, we set an (arbitrary) value of 10 overlapping beads between the two knots. If the free energy reaches a maximum before the intertwined state, as was the case in experiments,[25] then we could make a reliable estimate of E_s that is independent of the threshold choice for defining the intertwined state because the transition state value D_s^* is known. Unfortunately, as indicated in Fig. 4, the free energy increases monotonically up to the intertwined state. We thus have a lower bound for E_s, but the error in the actual value of E_s is uncontrolled because we do not have a measure of D_s^*. The impact of the ambiguity in the definition of an intertwined state is even more pernicious for E_i because the intertwined state in our analysis is counted as a single, degenerate state

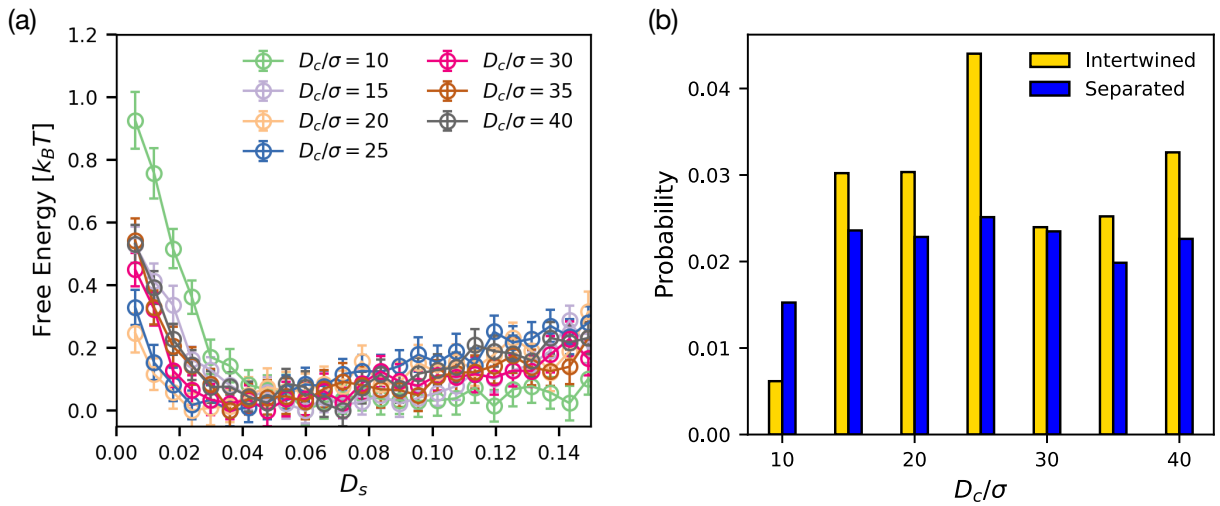

Figure 5: Impact of channel size on free energy and the probability of intertwining for a 3_1 knot. (a) Free energy profile as a function of knot-knot separation distance for different channel sizes for $D_s > 0$. The free energy curves are shifted to 0 based on the value of free energy at the most probable state of separation. (b) Probability for being in the intertwined state (yellow bar) or at the minimum free energy of the separated state (blue bar) for different channel sizes.

rather a continuum of states. For example, one could imagine a set of intertwined states that depend on the number of overlapping beads (e.g., by treating these as negative values of D_s) in a manner analogous to the distribution of D_s values when the knots are not intertwined. In such an alternate analysis, there would be a preferred number of overlapping beads for the intertwined state that would set the minimum value of the free energy of the intertwined state. By definition, this new minimum must be higher than the we might compute from Fig. 4 where any intertwined state is counted as $D_s = 0$. As a result, there is even more reason for concern in estimating a barrier height E_i.

Fortunately, the aforementioned concerns about estimating barrier heights prove unimportant for our analysis. Rather, we can understand the role of confinement on the interactions between the two knots by considering (i) the free energy for values $D_s > 0$, which are well defined, and (ii) the probability of observing the intertwined state at $D_s = 0$, which is also well defined, without having to draw a tenuous connection between the latter probability and a free energy. The results of this analysis appear in Fig. 5, where Fig. 5a provides the

free energy profiles for different nanochannel sizes and Fig. 5b provides the probability of being in the intertwined state and the probability of being located at the minimum in the free energy for $D_s > 0$.

The impact of channel size is apparent from the free energy and the probability data in Fig. 5. Channel sizes down to $D_c/\sigma = 15$ produce qualitatively similar free energy profiles. There is a long-range attraction towards an energy minimum in the separated state near $D_s = 0.05$. The extent of the attraction, i.e., the slope of the free energy for $D_s > 0.05$, exhibits a modest increase for these channel sizes. The results in Fig. 5a are starkly different for the smallest channel size, $D_c/\sigma = 10$. As the knots approach one another, there is a sharp increase in the free energy for $D_s < 0.05$ that differs significantly from that observed for the larger channel sizes. Likewise, the long-range attraction that was observed in the larger channel sizes becomes negligible for $D_c/\sigma = 10$, as indicated by the almost flat free energy profile for D_s values larger than the minimum for the separated state. Moreover, Fig. 5b also indicates a qualitative change in the results for the smallest channel size, $D_c/\sigma = 10$, when we considered the intertwined state. The probability of being located in the intertwined state is much lower compared to larger channel sizes, indicating that an inhibition of the two knot intertwining occurs in the smallest channel size, $D_c/\sigma = 10$.

While we can easily define the probability of observing the intertwined state in our simulation, at least to within the ambiguity surrounding the threshold for defining this state, it is less obvious what is meant by a "separated" state. For example, one could integrate the probability density over a region near the most probable separated state, but the definition of that region has a similar ambiguity to that defining the intertwined state. Likewise, if one simply considers separated states to be non-intertwined states, then the result would depend on the degree of polymerization of the polymer; for an infinitely long polymer, there are an infinite number of states where the two knots are sufficiently far apart to avoid any interactions, so the probability of being separated would tend to unity.

Nevertheless, we can make a simple argument by comparing the probability of observing

the intertwined state to probability corresponding to the most probable separated state, recognizing that our data are discrete since the value of D_s is computed from the number of beads between the two knots (Fig. 2). The results in Fig. 5b indicate a qualitative change in the results for $D_c/\sigma = 10$, with the probability of being located in the most probable separated value of D_s now being higher than the probability of locating the system in the intertwined state. Figure S3 further shows the short-time behavior of two knot attraction, which quantify the probability that two knots decreases in distance over a short time interval as a function of the knot separation distance. For $D_c/\sigma = 15$ to 40, two knots experience higher probability of attraction at larger separation distance, indicating a long-range attraction. Conversly, for $D_c/\sigma = 10$, two knots have a approximately equal probability of attraction or repulsion over short times, suggesting behavior akin to independent random walks.

The impact of small channel size is even more profound if we look into the details of the dynamics of the two knot intertwining. Figure S4 shows the cumulative probability of lifetimes for the intertwined states for different channel sizes. For larger channel size down to $D_c/\sigma = 15$, two knots can remain in the intertwined state for an extended period of time, where one knot enters, passes through, and exits the enlarged complex knot. This two knot behavior, as well as the duration of intertwined time, is analogous to the passing-though mechanisms observed in stretched polymers, where two knots remain in close contacts for more than a minute[26] and are able to pass through each other by swapping positions.[27] For smallest channel size at $D_c/\sigma = 10$, such passing through behavior is not observed. The longest time that two knots spent within the intertwined states from all replicates is only about $10^2\tau_{MD}$ as shown in Fig. S5. In this small channel size, two knots are more likely approach and leave the intertwined state quickly without any indication of moving along the enlarged knots or even swapping positions. This behavior is akin to the nanochannel experiments,[25] where two knots only remain closely for several seconds.

Discussion

The results obtained here raise two interrelated questions. The first question is relatively obvious, namely the origin of the distinctly different behavior observed for $D_c/\sigma = 10$ in Fig. 5. The second question is more subtle. The nanochannel experiments motivating our simulations[25] did not observe any intertwining of the two knots in a channel of $D_c = 300$ nm under an ionic strength that is mimicked by the polymer model used in our simulations. With $\sigma = 12$ nm, the experimental data indicate no intertwining for $D_c/\sigma = 25$, in clear contradiction with our simulation data. As we will see shortly, both questions can be addressed through a single analysis.

Let us begin with the more straightforward question of the change in behavior for $D_c/\sigma = 10$. We will consider two different hypotheses that could explain this result. The first arises from the standard theory for nanochannel confined DNA,[43] and posits that the result arises simply from a change in the confinement regime. The second considers the relative magnitude of the transverse fluctuations as the channel size decreases.

Based on the theory of nanochannel confined semiflexible polymers,[43,44] the channel size $D_c/\sigma = 25$ is the crossover between the extended de Gennes and de Gennes regimes, while the channel size $D_c/\sigma = 10$ is part of the transition to classical Odijk scaling; a backfolded Odijk regime is not observed for the moderate stiffness of DNA.[45] For channel sizes from $D_c/\sigma = 15$ to 40, two initially separated knots are capable of passing through each other and remaining intertwined for an extended period, similar to the example in Figure 3a. Conversely, in the smallest channel size, $D_c/\sigma = 10$, all simulation trajectories of knot-knot evolution show that the knots are unable to pass through one another; the trajectories are akin to Fig. 3c. These observations are consistent with the theory of confined DNA; if the channels are too small to allow for easy backfolding of the DNA, then the knots cannot swell sufficiently to allow pass-through. One could make a more detailed, quantitative analysis of this overall hypothesis in the context of the global persistence length of confined DNA,[45–47] which quantifies the typical length scale for hairpin formation in the channel and increases exponentially with

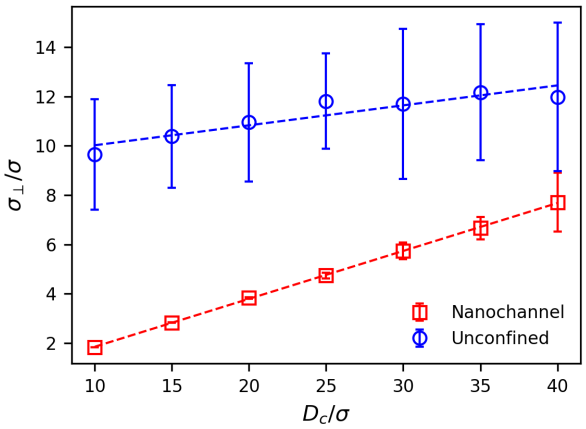

Figure 6: The transverse fluctuations as a function of nanochannel size for confined and stretched, unconfined double-knotted DNA molecules. For unconfined DNA, the value of D_c corresponds to DNA molecules that are stretched to the same end-to-end distance as one of the initial conditions used for the nanochannel-confined DNA in a channel of that size.

decreasing ratios D_c/l_p. However, that level of quantitation will prove unimportant in the context of our eventual conclusion regarding the validity of this hypothesis.

We have also quantified the degree of transverse fluctuations as a function of the nanochannel confinement. Several examples are provided in Fig. S6, along with plots of the cross-sectional probability distribution that are consistent with prior work.[42] Figure 6 summarizes the key results of this analysis, demonstrating a monotonic decrease in the magnitude of the transverse fluctuations as the channel size decreases, as would be expected by the cutoff imposed by the channel walls.[21,48] Figure 6 also provides equivalent data for unconfined DNA; we will return to these data shortly but they are not relevant for the present question of the change in behavior at $D_c/\sigma = 10$. For the moment, the key message in Fig. 6 is that one could make a plausible argument that the transverse fluctuations are sufficiently suppressed for $D_c/\sigma = 10$ that one of the trefoil knots can no longer swell to a sufficient extent to allow the second knot to enter it, thereby suppressing the intertwining.

We thus have two plausible arguments, one based on the ability of the chain to bend within the channel, and another based on the magnitude of the transverse fluctuations, that are both consistent with the observed behavior in Fig. 5. To distinguish between these

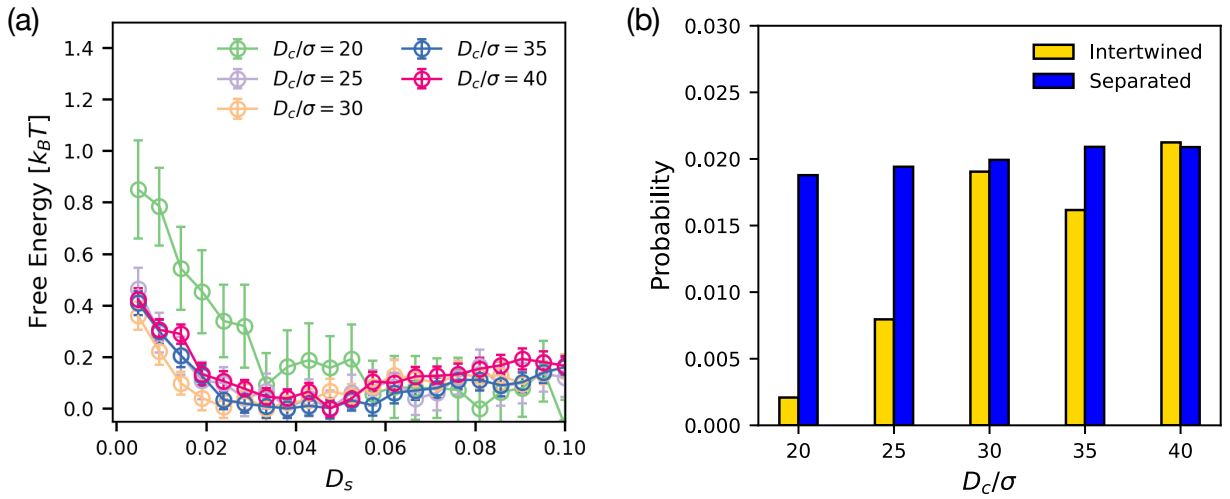

Figure 7: Same as Fig. 5 but now for a 4_1 knot. (a) Free energy profile as a function of 4_1 knot-knot separation distance for different channel sizes for $D_s > 0$. The free energy curves are shifted to 0 based on the value of free energy at the most probable state of separation. (b) Probability for being in the intertwined state (yellow bar) or at the minimum free energy of the separated state (blue bar) for different channel sizes.

two possibilities, we decided to perform additional simulations of two 4_1 knots in the same nanochannels. If the confinement-regime hypothesis is correct, and intertwining of the chains is controlled by hairpin formation, then we would expect the suppression of knot intertwining to persist at $D_c/\sigma = 10$. In contrast, if the hypothesis about knot swelling is correct, then larger transverse fluctuations will be required to intertwine the more complicated 4_1 knots than was required for the simple 3_1 trefoil knots. In this case, we would expect that intertwining to be suppressed for some channel size $D_c/\sigma > 10$.

Figure 7 provides the free energy and intertwining probabilities for the 4_1 knot that can be compared to similar data in Fig. 5 for the 3_1 knot. To generate the data in Fig. 7, we started with the largest channel size used for the trefoil knot and continued to decrease the channel size until we observed a suppression of intertwining of the 4_1 knot that is akin to what we found for the 3_1 knot at $D_c/\sigma = 10$. Remarkably, the intertwining is already suppressed for $D_c/\sigma = 25$. As a result, we conclude that the hypothesis based on transverse fluctuations is the better explanation of the ability for two channel-confined knots to become intertwined.

The data in Fig. 7 also provide an explanation for the apparent discrepancy between the extensive data set we acquired for the interactions between two trefoil knots in Fig. 5 and the experimental data for a 300 nm nanochannel.[25] The knot factory likely produces complex knots,[9] and it is reasonable to anticipate that many of the two-knot experimental data[25] correspond to knots that are even more complex than the 4_1 knot. For sure, the knots in the experimental data are generally more complex than the simple 3_1 knot. We already know from Fig. 7 that going one step up in knot complexity to the 4_1 knot starts to suppress intertwining at $D_c/\sigma = 25$, consistent with the 300 nm channel data.[25] It is very likely that the suppression of transverse fluctuations in a 300 nm nanochannel are sufficient to eliminate knot intertwining for all knots that are more complex than a trefoil knot, at least to within the amount of data that can be acquired on a realistic experimental budget. However, we have not engaged in a systematic study of more complex knots to quantify this point via simulation, and there is no direct method to measure the knot complexity in experiments. We thus leave this point as a plausible, but not yet proven, conjecture.

At the outset of our discourse, we also raised a question about the difference between knots under tension, where the two knots in close proximity and intertwining is frequently observed,[26–30] and the suppression of intertwining in nanochannels. Our hypothesis that the emergence of intertwining is connected to a sufficient degree of transverse fluctuations is also consistent with this difference between the two systems. To be quantitative, we computed the transverse fluctuations for unconfined DNA with two trefoil knots. To do so, we started from at least 300 of the initial chain configurations that we used for given channel size D_c, tethered the two end beads near their initial position (Eq. 8), and then removed the wall potential (Eq. 5); this ensemble of simulations is denoted as having an equivalent nanochannel size $D_c^* = D_c$, where the asterisk is used to distinguish the free solution simulation from a confined simulation. This approach maintains a similar chain extension and its variance even when the wall is removed (Fig. S2).

Figure 8 demonstrates that intertwining takes place for all degrees of stretching in solu-

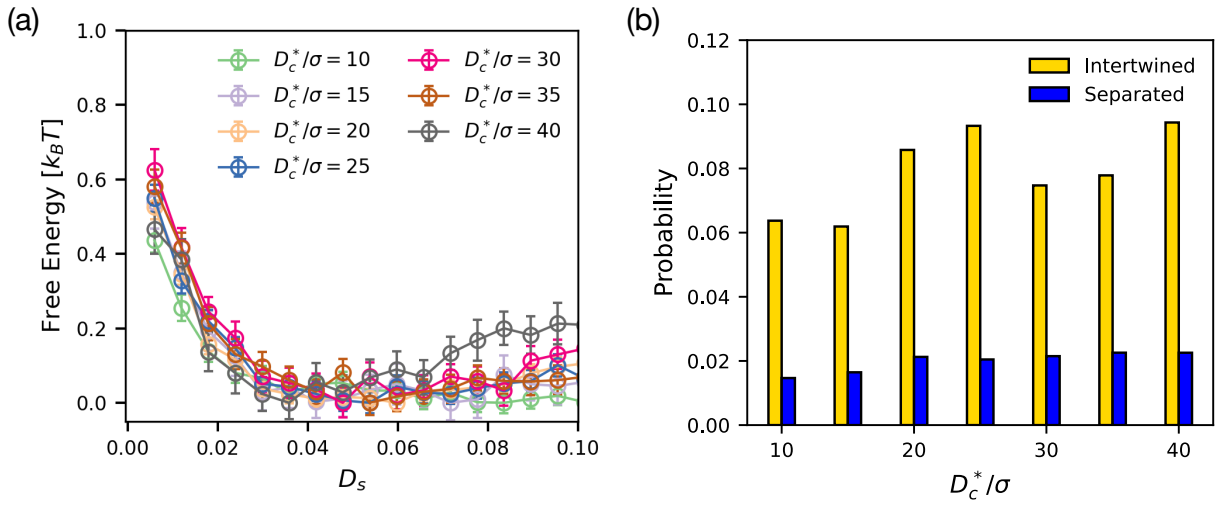

Figure 8: Free energy and the probability of intertwining of unconfined, double-knotted DNA molecules. The quantity D_c^*/σ represents the channel size used to obtain initial configurations for the free-solution simulations with the two terminal beads tethered near their initial positions. (a) Free energy profile as a function of knot-knot separation distance for different D_c^*/σ for $D_s > 0$. The free energy curves are shifted to 0 based on the value of free energy at the most probable state of separation. (b) Probability for being in the intertwined state (yellow bar) or at the minimum free energy of the separated state (blue bar) for different D_c^*/σ.

tion, even when we have imposed a degree of stretching that is consistent with the extension that we observed in the $D_c/\sigma = 10$ nanochannel; Fig. S7 provides a companion to Fig. 3 illustrating the intertwining of a two knots in the absence of confinement. Indeed, not only is intertwining observed for all values of D_c^*, but the free energies are also relatively insensitive to the degree of stretching.

The results in Fig. 8 can be explained by the magnitude of the transverse fluctuations. Figure S8 provides examples of the transverse fluctuations for the unconfined chains. As we might expect, the tethering of the end beads constrains their transverse fluctuations to the spherical shell corresponding to the energy minimum created by the spring force in Eq. 8. However, the midpoint of the chain can experience very large transverse fluctuations because the stretching is not very strong. Returning to the data for the magnitude of the transverse fluctuations in Fig. 6, we see that $\sigma_\perp$ is only weakly impacted by the stretching of an unconfined chain. If transverse fluctuations control the extent of intertwining, then we

would expect that the probability of intertwining is relatively insensitive to D_c^*, which is what is observed in Fig. 8. If we further use the nanochannel data to postulate that intertwining of a 3_1 knot is suppressed only when the magnitude of the transverse fluctuations is below $\sigma_\perp = 2\sigma$, it becomes apparent that a very high degree of stretching would be required to reach this limit.[49]

Conclusions

Our findings lead us to conclude that the magnitude of the transverse fluctuations plays a key role governing the intertwining of two knots along a DNA molecule. In solution, a modestly stretched DNA molecule is able to experience large transverse fluctuations far from the tether point, which permits intertwining. When a DNA molecule is instead extended via compression in a nanochannel, the cutoff of the transverse fluctuations from the nanochannel walls may suppress the ability of two knots to intertwine. For a trefoil 3_1 knot, the onset of this suppression is coincident with lower bound in the channel size for the transition from the extended de Gennes regime to the classical Odijk regime. While this observation may lead one to suspect that the suppression of knot intertwining is connected to the rapid increase in the global persistence length for this small channel size,[45–47] further analysis of the intertwining of a 4_1 knot shows that suppression of the intertwining knots now takes place at a larger channels size. The identification of polymer transverse fluctuations as the key factor controlling knot intertwining allows us to reconcile seemingly disparate results obtained for polymers stretched in solution and those in nanochannel confinement.

Acknowledgments

This work was supported by National Science Foundation through award CBET-2016879. Computational resources were provided by the Minnesota Supercomputing Institute.

Supporting Information

Histogram of the minimum distance for each simulation trajectory for $D/\sigma = 40$; comparison of the average and variance in the extension for confined and unconfined chains; probability of attraction between knots; cumulative probability distribution for the knot lifetimes; trajectory for $D_c/\sigma = 10$ with the maximum observed intertwining; examples of the transverse fluctuations and cross-sectional distributions for confined chains; illustration of a trajectory for intertwining of an unconfined chain; examples of the transverse fluctuations and cross-sectional distributions for stretched, unconfined chains.

References

(1) Orlandini, E. Statics and dynamics of DNA knotting. *J. Phys. A* **2017**, *51*, 053001.

(2) Dai, L.; Renner, C. B.; Doyle, P. S. The polymer physics of single DNA confined in nanochannels. *Adv. Colloid Interface Sci.* **2016**, *232*, 80–100.

(3) Shaqfeh, E. S. The dynamics of single-molecule DNA in flow. *J. Non-Newton. Fluid Mech.* **2005**, *130*, 1–28.

(4) Arai, Y.; Yasuda, R.; Akashi, K.-i.; Harada, Y.; Miyata, H.; Kinosita Jr, K.; Itoh, H. Tying a molecular knot with optical tweezers. *Nature* **1999**, *399*, 446–448.

(5) Bao, X. R.; Lee, H. J.; Quake, S. R. Behavior of Complex Knots in Single DNA Molecules. *Phys. Rev. Lett.* **2003**, *91*, 265506.

(6) Soh, B. W.; Klotz, A. R.; Doyle, P. S. Untying of Complex Knots on Stretched Polymers in Elongational Fields. *Macromolecules* **2018**, *51*, 9562–9571.

(7) Narsimhan, V.; Klotz, A. R.; Doyle, P. S. Steady-State and Transient Behavior of Knotted Chains in Extensional Fields. *ACS Macro Lett.* **2017**, *6*, 1285–1289.

(8) Klotz, A. R.; Narsimhan, V.; Soh, B. W.; Doyle, P. S. Dynamics of DNA knots during chain relaxation. *Macromolecules* **2017**, *50*, 4074–4082.

(9) Amin, S.; Khorshid, A.; Zeng, L.; Zimny, P.; Reisner, W. A nanofluidic knot factory based on compression of single DNA in nanochannels. *Nat. Commun.* **2018**, *9*, 1506.

(10) Liu, L. F.; Perkocha, L.; Calendar, R.; Wang, J. C. Knotted DNA from bacteriophage capsids. *Proc. Natl. Acad. Sci. USA* **1981**, *78*, 5498–5502.

(11) Meluzzi, D.; Smith, D. E.; Arya, G. Biophysics of knotting. *Annu. Rev. Biophys.* **2010**, *39*, 349–366.

(12) Rybenkov, V. V.; Cozzarelli, N. R.; Vologodskii, A. V. Probability of DNA knotting and the effective diameter of the DNA double helix. *Proc. Natl. Acad. Sci. USA* **1993**, *90*, 5307–5311.

(13) Sumners, D.; Whittington, S. Knots in self-avoiding walks. *J. Phys. A* **1988**, *21*, 1689–1694.

(14) O'Donnol, D.; Stasiak, A.; Buck, D. Two convergent pathways of DNA knotting in replicating DNA molecules as revealed by θ-curve analysis. *Nucleic Acids Res.* **2018**, *46*, 9181–9188.

(15) Olavarrieta, L.; Martínez-Robles, M. L.; Hernandez, P.; Krimer, D. B.; Schvartzman, J. B. Knotting dynamics during DNA replication. *Mol. Microbiol.* **2002**, *46*, 699–707.

(16) Chen, S. H.; Chan, N.-L.; Hsieh, T.-s. New mechanistic and functional insights into DNA topoisomerases. *Annu. Rev. Biochem.* **2013**, *82*, 139–170.

(17) Lam, E. T.; Hastie, A.; Lin, C.; Ehrlich, D.; Das, S. K.; Austin, M. D.; Deshpande, P.; Cao, H.; Nagarajan, N.; Xiao, M.; Kwok, P.-Y. Genome mapping on nanochannel

arrays for structural variation analysis and sequence assembly. *Nat. Biotechnol.* **2012**, *30*, 771–776.

(18) Jain, A.; Dorfman, K. D. Simulations of knotting of DNA during genome mapping. *Biomicrofluidics* **2017**, *11*, 024117.

(19) Ma, Z.; Dorfman, K. D. Diffusion of knots along DNA confined in nanochannels. *Macromolecules* **2020**, *53*, 6461–6468.

(20) Mao, R.; Dorfman, K. D. Diffusion of knots in nanochannel-confined DNA molecules. *J. Chem. Phys.* **2023**, *158*, 194901.

(21) Dai, L.; Doyle, P. S. Comparisons of a polymer in confinement versus applied force. *Macromolecules* **2013**, *46*, 6336–6344.

(22) Rieger, F. C.; Virnau, P. A Monte Carlo study of knots in long double-stranded DNA chains. *PLoS Comput. Biol.* **2016**, *12*, e1005029.

(23) Plesa, C.; Verschueren, D.; Pud, S.; van der Torre, J.; Ruitenberg, J. W.; Witteveen, M. J.; Jonsson, M. P.; Grosberg, A. Y.; Rabin, Y.; Dekker, C. Direct Observation of DNA Knots Using a Solid-State Nanopore. *Nat. Nanotechnol.* **2016**, *11*, 1093–1097.

(24) Kumar Sharma, R.; Agrawal, I.; Dai, L.; Doyle, P. S.; Garaj, S. Complex DNA knots detected with a nanopore sensor. *Nat. Commun.* **2019**, *10*, 4473.

(25) Ma, Z.; Dorfman, K. D. Interactions between two knots in nanochannel-confined DNA molecules. *J. Chem. Phys.* **2021**, *155*, 154901.

(26) Klotz, A. R.; Soh, B. W.; Doyle, P. S. An experimental investigation of attraction between knots in a stretched DNA molecule. *Europhys. Lett.* **2020**, *129*, 68001.

(27) Trefz, B.; Siebert, J.; Virnau, P. How molecular knots can pass through each other. *Proc. Natl. Acad. Sci. USA* **2014**, *111*, 7948–7951.

(28) Najafi, S.; Tubiana, L.; Podgornik, R.; Potestio, R. Chirality modifies the interaction between knots. *Europhys. Lett.* **2016**, *114*, 50007.

(29) Najafi, S.; Podgornik, R.; Potestio, R.; Tubiana, L. Role of Bending Energy and Knot Chirality in Knot Distribution and Their Effective Interaction along Stretched Semiflexible Polymers. *Polymers* **2016**, *8*, 347.

(30) Richard, D.; Stalter, S.; Siebert, J. T.; Rieger, F.; Trefz, B.; Virnau, P. Entropic Interactions between Two Knots on a Semiflexible Polymer. *Polymers* **2017**, *9*, 55.

(31) Tree, D. R.; Muralidhar, A.; Doyle, P. S.; Dorfman, K. D. Is DNA a Good Model Polymer? *Macromolecules* **2013**, *46*, 8369–8382.

(32) Persson, F.; Utko, P.; Reisner, W.; Larsen, N. B.; Kristensen, A. Confinement Spectroscopy: Probing Single DNA Molecules with Tapered Nanochannels. *Nano Lett.* **2009**, *9*, 1382–1385.

(33) Gupta, D.; Sheats, J.; Muralidhar, A.; Miller, J. J.; Huang, D. E.; Mahshid, S.; Dorfman, K. D.; Reisner, W. Mixed Confinement Regimes during Equilibrium Confinement Spectroscopy of DNA. *J. Chem. Phys.* **2014**, *140*, 214901.

(34) Frykholm, K.; Müller, V.; Sriram, K.; Dorfman, K. D.; Westerlund, F. DNA in Nanochannels: Theory and Applications. *Quart. Rev. Biophys.* **2022**, *55*, e12.

(35) Werner, E.; Mehlig, B. Scaling Regimes of a Semiflexible Polymer in a Rectangular Channel. *Phys. Rev. E* **2015**, *91*, 050601.

(36) Grosberg, A. Y.; Rabin, Y. Metastable Tight Knots in a Wormlike Polymer. *Phys. Rev. Lett.* **2007**, *99*, 217801.

(37) Grest, G. S.; Kremer, K. Molecular dynamics simulation for polymers in the presence of a heat bath. *Phys. Rev. A* **1986**, *33*, 3628–3631.

(38) Weeks, J. D.; Chandler, D.; Andersen, H. C. Role of repulsive forces in determining the equilibrium structure of simple liquids. *J. Chem. Phys.* **1971**, *54*, 5237–5247.

(39) Scharein, R. G. Interactive topological drawing. Ph.D. thesis, University of British Columbia, 1998.

(40) Thompson, A. P.; Aktulga, H. M.; Berger, R.; Bolintineanu, D. S.; Brown, W. M.; Crozier, P. S.; in't Veld, P. J.; Kohlmeyer, A.; Moore, S. G.; Nguyen, T. D.; Shan, R.; Stevens, M. J.; Tranchida, J.; Trott, C.; Plimpton, S. J. LAMMPS-a flexible simulation tool for particle-based materials modeling at the atomic, meso, and continuum scales. *Comput. Phys. Commun.* **2022**, *271*, 108171.

(41) Tubiana, L.; Polles, G.; Orlandini, E.; Micheletti, C. Kymoknot: A web server and software package to identify and locate knots in trajectories of linear or circular polymers. *Eur. Phys. J. E* **2018**, *41*, 72.

(42) Reinhart, W. F.; Tree, D. R.; Dorfman, K. D. Entropic Depletion of DNA in Triangular Nanochannels. *Biomicrofluidics* **2013**, *7*, 024102.

(43) Odijk, T. Scaling Theory of DNA Confined in Nanochannels and Nanoslits. *Phys. Rev. E* **2008**, *77*, 060901(R).

(44) Wang, Y.; Tree, D. R.; Dorfman, K. D. Simulation of DNA Extension in Nanochannels. *Macromolecules* **2011**, *44*, 6594–6604.

(45) Muralidhar, A.; Tree, D. R.; Dorfman, K. D. Backfolding of Wormlike Chains Confined in Nanochannels. *Macromolecules* **2014**, *47*, 8446–8458.

(46) Odijk, T. DNA Confined in Nanochannels: Hairpin Tightening by Entropic Depletion. *J. Chem. Phys.* **2006**, *125*, 204904.

(47) Chen, J. Z. Y. Conformational Properties of a Back-Folding Wormlike Chain Confined in a Cylindrical Tube. *Phys. Rev. Lett.* **2017**, *118*, 247802.

(48) Yeh, J.-W.; Taloni, A.; Sriram, K.; Shen, J.-P.; Kao, D.-Y.; Chou, C.-F. Nanoconfinement-Induced DNA Reptating Motion and Analogy to Fluctuating Interfaces. *Macromolecules* **2020**, *53*, 1001–1013.

(49) Marko, J. F.; Siggia, E. D. Stretching DNA. *Macromolecules* **1995**, *28*, 8759–8770.